NANO LETTERS

Letter

pubs.acs.org/NanoLett

High-Energy All-Solid-State Lithium Batteries with Ultralong Cycle Life

Xiayin Yao,[†] Deng Liu,[†] Chunsheng Wang,[‡] Peng Long,[†] Gang Peng,[†] Yong-Sheng Hu,[*,§] Hong Li,[§] Liquan Chen,[§] and Xiaoxiong Xu[*,†]

[†]Ningbo Institute of Materials Technology and Engineering, Chinese Academy of Sciences, Ningbo 315201, P. R. China

[‡]Department of Chemical and Biomolecular Engineering, University of Maryland, College Park, Maryland 20742, United States

[§]Key Laboratory for Renewable Energy, Beijing Key Laboratory for New Energy Materials and Devices, Beijing National Laboratory for Condensed Matter Physics, Institute of Physics, Chinese Academy of Sciences, Beijing 100190, P. R. China

Supporting Information

ABSTRACT: High energy and power densities are the greatest challenge for all-solid-state lithium batteries due to the poor interfacial compatibility between electrodes and electrolytes as well as low lithium ion transfer kinetics in solid materials. Intimate contact at the cathode−solid electrolyte interface and high ionic conductivity of solid electrolyte are crucial to realizing high-performance all-solid-state lithium batteries. Here, we report a general interfacial architecture, i.e., $Li_7P_3S_{11}$ electrolyte particles anchored on cobalt sulfide nanosheets, by an in situ liquid-phase approach. The anchored $Li_7P_3S_{11}$ electrolyte particle size is around 10 nm, which is the smallest sulfide electrolyte particles reported to date, leading to an increased contact area and intimate contact interface between electrolyte and active materials. The neat $Li_7P_3S_{11}$ electrolyte synthesized by the same liquid-phase approach exhibits a very high ionic conductivity of 1.5×10^{-3} S cm^{-1} with a particle size of 0.4−1.0 μm. All-solid-state lithium batteries employing cobalt sulfide−$Li_7P_3S_{11}$ nanocomposites in combination with the neat $Li_7P_3S_{11}$ electrolyte and Super P as the cathode and lithium metal as the anode exhibit excellent rate capability and cycling stability, showing reversible discharge capacity of 421 mAh g^{-1} at 1.27 mA cm^{-2} after 1000 cycles. Moreover, the obtained all-solid-state lithium batteries possesses very high energy and power densities, exhibiting 360 Wh kg^{-1} and 3823 W kg^{-1} at current densities of 0.13 and 12.73 mA cm^{-2}, respectively. This contribution demonstrates a new interfacial design for all-solid-state battery with high performance.

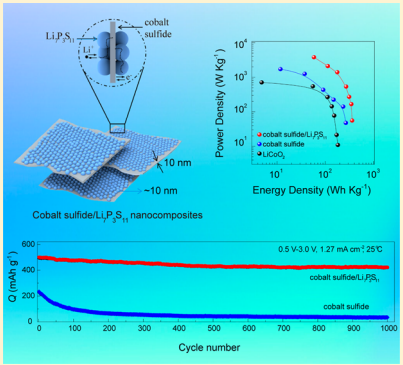

KEYWORDS: *All-solid-state lithium battery, interfacial architecture, sulfide electrolyte, cobalt sulfide−$Li_7P_3S_{11}$ nanocomposites, cycling stability*

Currently commercialized lithium ion batteries generally suffer from serious safety arising from their flammable organic liquid electrolytes.[1,2] All-solid-state lithium batteries, using inorganic solid electrolytes instead of combustible liquid electrolytes, are considered to be the ultimate solution to address this issue.[3,4] Meanwhile, the energy density of the all-solid-state lithium battery could be further improved by using a lithium metal as anode, making it a novel candidate for large scale energy storage devices or electric vehicle and hybrid electric vehicle power sources.[5,6]

All-solid-state lithium batteries, employing sulfide solid electrolytes and conventional layered or spinel lithium transition-metal oxides as cathodes,[7,8] are extensively investigated due to the rapid development of sulfide electrolytes with high ionic conductivity of 10^{-2} to 10^{-3} S cm^{-1} and chemical stability.[2,9−11] The energy density for the all-solid-state lithium battery using $LiCoO_2$ as a positive material has reached the level comparable to that of liquid one.[8] However, it is still far from meeting the demand for the electric vehicle and hybrid electric vehicle applications due to its theoretical specific capacity limitation. Moreover, power density and cycling stability remain an obstacle for an all-solid-state lithium battery to be practically applied, owing to a large interfacial resistance between the cathode and sulfide electrolyte.[12,13] This issue can be somewhat alleviated by introducing an electron-insulating and ion-conducting material as a functional buffer layer at the active material and sulfide electrolyte interface.[8,12−14] Consequently, favorable and stable solid−solid interfaces between electrodes and solid electrolytes are crucial to achieving excellent electrochemistry performances. Thus far, it is indispensable to develop electrode materials possessing wonderful compatibility with solid electrolytes as well as high charge−discharge capacities for all-solid-state lithium batteries.

Recently, transition metal sulfides have captured much attention due to their favorable interface compatibility with sulfide electrolytes as well as high theoretical capacity, moderate

Received: August 16, 2016
Revised: October 4, 2016
Published: October 21, 2016

DOI: 10.1021/acs.nanolett.6b03448
Nano Lett. 2016, 16, 7148−7154

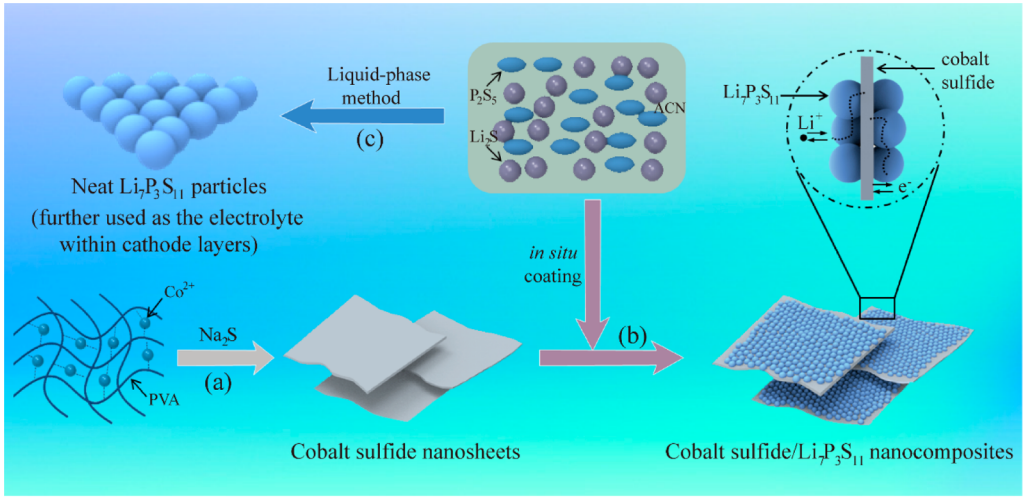

Figure 1. Schematic illustration of the synthesis strategy for (a) cobalt sulfide, (b) cobalt sulfide−$Li_7P_3S_{11}$ nanocomposites, and (c) neat $Li_7P_3S_{11}$ electrolyte.

operating voltage, and chemical stability.[15−17] In particular, the energy density can be further improved by reducing particle sizes of active materials. However, intimate contact between nanosized active materials and micron-sized sulfide electrolytes will be a great challenge, which is also the main source for the interfacial resistances and stability. One strategy is to reduce the particle size of sulfide electrolytes as well. Liu et al.[18] have reported a liquid-phase method to synthesize nanoporous β-Li_3PS_4 with high lithium ionic conductivity in the order of 10^{-4} S cm^{-1}. This opens up the possibility for reducing the particle size of sulfide electrolytes. However, the lithium ionic conductivity of 10^{-4} S cm^{-1} needs to be further enhanced to meet the all-solid-state lithium battery applications. To pursue intimate interface contact, the nanosized sulfide electrolyte layer should be directly coated on the surface of active materials.[17,19] A highly ion-conducting Li_2S−P_2S_5 solid elctrolyte has been coated onto NiS-vapor-grown carbon fiber composite using pulsed laser deposition.[17] However, this method generally requires large-scale equipment and relatively complicated experimental procedures and is not easy to be scaled up. Therefore, it is extremely urgent to develop a simple and efficient method for constructing intimate interface contact between active materials and sulfide elctrolytes.

In this work, a novel interfacial architecture, i.e., ∼10 nm $Li_7P_3S_{11}$ electrolyte particles anchored on cobalt sulfide nanosheets, is achieved by an in situ liquid-phase appraoch. The unique strcuture endows an intimate contact interface and uniform volume changes of cobalt sulfide nanosheets, leading to an ultrastable all-solid-state lithium battery with excellent rate capability and cycling stability. The synthesis route for cobalt sulfide−$Li_7P_3S_{11}$ nanocomposites is illustrated in Figure 1. First, cobalt sulfide nanosheets are synthesized through a poly(vinyl alcohol) (PVA)-assisted aqueous precipitation reaction (Figure 1a). The main diffraction peaks in the X-ray diffraction (XRD) pattern for the as-synthesized cobalt sulfide are at 2θ = 15.4°, 29.8°, 31.2° and 52.0° (Figure 2a), which are corresponding to the diffraction from the (111), (311), (222), and (440) planes of the standard cubic-phase Co_9S_8 (JCPDS card no. 65-1765).[20] Scanning electron microscopy (SEM) and transmission electron microscopy (TEM) results show that cobalt sulfide has a nanosheet morphology with a lateral size of several hundred nanometers and thickness of around 10 nm (Figure S1a,b). High-resolution transmission electron microscopy (HRTEM) measurement further confirms the formation of Co_9S_8 crystal (Figure S1c).

With cobalt sulfide nanosheets and Li_2S and P_2S_5 (the mole ratio of Li_2S and P_2S_5 is 7:3) taken as the starting materials, an in situ liquid-phase deposition reaction occurs in an acetonitrile solvent, resulting in the cobalt sulfide−$Li_7P_3S_{11}$ nanocomposites precursor. Upon annealing at 260 °C, the deposited electrolyte precursor transfers to $Li_7P_3S_{11}$ crystal (Figure 1b). All diffraction peaks of cobalt sulfide−$Li_7P_3S_{11}$ nanocomposites can be ascribed to both cobalt sulfide and $Li_7P_3S_{11}$ electrolyte (Figure 2a). SEM studies show that the cobalt sulfide−$Li_7P_3S_{11}$ nanocomposites retain the nanosheet morphology of cobalt sulfide, and a significant $Li_7P_3S_{11}$ electrolyte layer uniformly grows on the surface of cobalt sulfide nanosheets (Figure 2b). The $Li_7P_3S_{11}$ electrolyte particles closely pack together (Figure S2a), which would be favorable for forming an intimate and stable solid−solid contact interface. As revealed by the TEM, the $Li_7P_3S_{11}$ electrolyte particles with an average size of around 10 nm homogeneously anchored on both side of cobalt sulfide nanosheets (Figures 2c and S2b,c). To the best of our knowledge, this would be the smallest sulfide electrolyte particles reported to date. The HRTEM image in Figure 2d shows clear lattices with interplanar distances of 0.299 and 0.574 nm and 0.290 and 0.304 nm, matching well with the d_{311}, d_{111} and d_{1-33}, d_{2-1-1} spacing of cobalt sulfide and $Li_7P_3S_{11}$ electrolyte, respectively. The selected area electron diffraction (SAED) pattern of the cobalt sulfide−$Li_7P_3S_{11}$ nanocomposites presents intense diffraction rings for both cobalt sulfide and $Li_7P_3S_{11}$ electrolyte (Figure 2e), which agrees well with the XRD and HRTEM results. Furthermore, the STEM-EDS elemental mapping of an individual nanocomposite in Figure 2f also confirms that the cobalt sulfide−$Li_7P_3S_{11}$ nanocomposites contain cobalt, sulfur, and phosphorus, and all elements are homogeneously distributed throughout the nanosheets.

For comparison, neat $Li_7P_3S_{11}$ electrolyte was synthesized (Figure 1c) and further used as electrolyte within the cathode layer in the all-solid-state batteries. XRD and Raman measurements confirm the simple crystal structure of $Li_7P_3S_{11}$ (Figures 2a and S3). Actually, the annealing temperature is crucial for obtaining the pure phase and high ionic conductivity. A too-high annealing temperature would form an impurity phase of

DOI: 10.1021/acs.nanolett.6b03448
Nano Lett. 2016, 16, 7148−7154

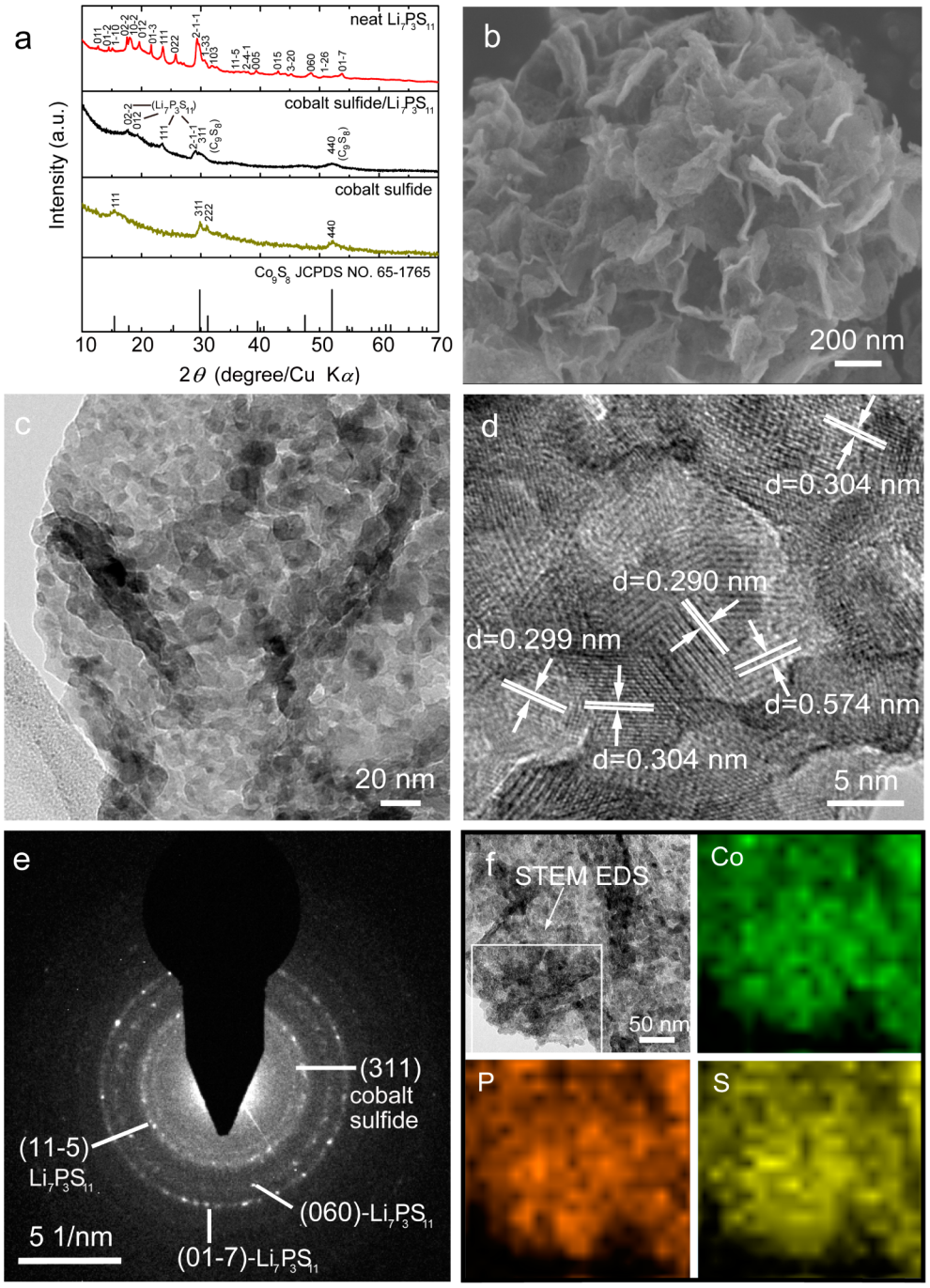

Figure 2. (a) XRD patterns of cobalt sulfide, cobalt sulfide−$Li_7P_3S_{11}$ nanocomposites, and neat $Li_7P_3S_{11}$ electrolyte; the standard Co_9S_8 JCPDS card is also shown. (b) SEM, (c) TEM, and (d) HRTEM images, (e) SEAD pattern, and (f) STEM EDS elemental mapping images of cobalt sulfide−$Li_7P_3S_{11}$ nanocomposites, marked by the rectangle region, for Co, S, and P.

$Li_4P_2S_6$, while low heat-treatment temperature was difficult to remove the cocrystallized acetonitrile molecules (Figure S4). Before annealing, the ionic conductivity of the neat $Li_7P_3S_{11}$ electrolyte precursor is only 5.35×10^{-5} S cm^{-1}. Upon annealing at optimized temperature of 260 °C for 1 h, the synthesized neat $Li_7P_3S_{11}$ electrolyte possesses a very high lithium ion conductivity of 1.5×10^{-3} S cm^{-1} with a low activation energy of 23 kJ mol^{-1} at room temperature (Figures S5 and S6 and Table S1), which are the best values in the reported references[18,21,22] and make it a promising solid electrolyte for $LiCoO_2$-based all-solid-state lithium batteries (Figure S7). SEM results show that the neat $Li_7P_3S_{11}$ electrolyte particles are fairly homogeneous and regular with the size distribute in the range of 0.4−1 μm (Figure S8). Clearly, compared with neat $Li_7P_3S_{11}$ electrolyte, the $Li_7P_3S_{11}$ electrolytes grown on the cobalt sulfide nanosheets possess extreme smaller particle size, which can be attributed to a nucleation and an impeding effects of cobalt sulfide nanosheets during its nucleation and growth process, inhibiting aggregation of newly formed electrolyte precursor nanoparticles.[23]

The electrochemical performances were investigated using laboratory-scale all-solid-state lithium cells (Figure S9), in which the neat $Li_7P_3S_{11}$ and super P are used as electrolyte and electronic additive in the cathode layer to achieve both high

DOI: 10.1021/acs.nanolett.6b03448
Nano Lett. 2016, 16, 7148−7154

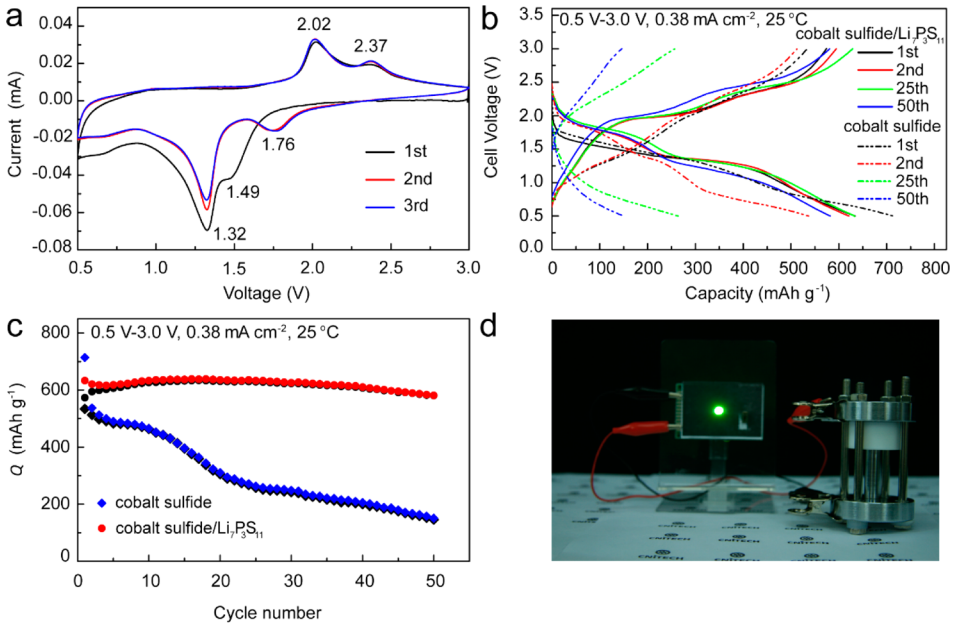

Figure 3. (a) Cyclic voltammograms of the cobalt sulfide−$Li_7P_3S_{11}$ nanocomposites. (b) Galvanostatic charge−discharge profiles and (c) cycle performances of the cobalt sulfide−$Li_7P_3S_{11}$ nanocomposite and cobalt sulfide nanosheet electrodes discharged and charged at a constant current density of 0.38 mA cm^{-2}. (d) A green LED powered by the prototype cell using cobalt sulfide−$Li_7P_3S_{11}$ nanocomposites.

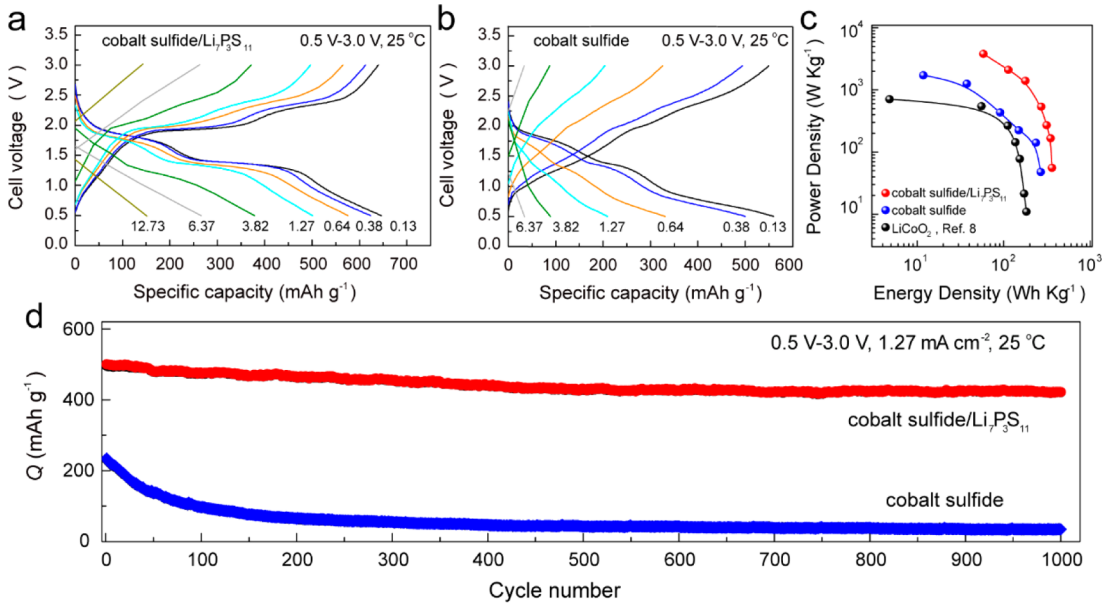

Figure 4. Discharge−charge curves of the cells using (a) cobalt sulfide−$Li_7P_3S_{11}$ nanocomposite electrode and (b) cobalt sulfide nanosheet electrode at various current densities (mA cm^{-2}). (c) Ragone plots. The plots were derived from the discharge curves in (a) and (b). (d) Cycling stability at current density of 1.27 mA cm^{-2}.

ionic and electronic conduction, while the $Li_{10}GeP_2S_{12}$/70% Li_2S−29% P_2S_5−1% P_2O_5 bilayer were used as the electrolyte in the solid-state cell to increase the ionic conduction and stability to lithium anode. As shown in the cyclic voltammetry (CV) curves (Figure 3a), the peak at around 1.49 V in the first cathodic scan can be attributed to the Li insertion into Co_9S_8 to form $Li_xCo_9S_8$, and it shifts to the positive voltage of 1.76 V for the subsequent scans, which suggests the decreased electrode polarization due to the structure rearrangement and favorable lithium ion conduction paths at the interface between electrode material and electrolyte layer.[24] A sharp peak at about 1.32 V is related to the electrochemical conversion reaction, forming cobalt metal and lithium sulfide. In the anodic scan, two obvious peaks at 2.02 and 2.37 V were recorded, corresponding to oxidation reaction of cobalt metal back to $Li_xCo_9S_8$ and the extraction reaction of Li^+ ions, respectively.[24] The overall electrochemical processed can be expressed as $Co_9S_8 + 16Li^+ + 16e^- \rightleftharpoons 9Co + 8Li_2S$.[20,25] From the second cycle onward, the CV curves almost overlap, indicating the stable and superior reversibility of cobalt sulfide−$Li_7P_3S_{11}$ nanocomposites in the all-solid-state lithium cell.

The galvanostatic charge−discharge profiles of cobalt sulfide−$Li_7P_3S_{11}$ nanocomposites at 0.38 mA cm^{-2} in voltage window of 0.5−3.0 V (versus Li/Li^+) are shown in Figure 3b.

DOI: 10.1021/acs.nanolett.6b03448
Nano Lett. 2016, 16, 7148−7154

The plateaux observed in the discharge−charge curves are consistent with the peaks in CV analysis mentioned above. The cobalt sulfide−$Li_7P_3S_{11}$ nanocomposite electrode delivers an initial specific discharge capacity of 633 mAh g^{-1} and a reversible charge capacity of 574 mAh g^{-1} with a high Coulombic efficiency of 90.7%, which is much higher than that of nanosized conversion electrodes in liquid electrolyte lithium ion batteries.[26] The high Coulombic efficiency could be benefit from the intimate contact interface between active material and sulfide electrolyte and less side reaction between cobalt sulfide and $Li_7P_3S_{11}$. After the first discharge process, the discharge product Li_2S can still tightly contact with electrolyte, keeping electrochemically reversible, leading to high active mass utilization with markedly improved Coulombic efficiency.[27] From the second cycle onward, the cobalt sulfide−$Li_7P_3S_{11}$ nanocomposite electrode shows excellent cycling stability, exhibiting a reversible specific capacity of 582 mAh g^{-1} with a capacity retention of 91.9% after 50 cycles (Figure 3c). However, the cobalt sulfide nanosheet electrode presents no obvious plateau and severe polarization in the subsequent cycles (Figure 3b). Compared with cobalt sulfide−$Li_7P_3S_{11}$ nanocomposite electrode, the poor contact between Li_2S and electrolyte after the first discharge could lead to electrochemically inaccessible of partial noncontact Li_2S, causing a poor active material utilization and uneven volume change, thus high local stress−strain and low Coulombic efficiency. Also, it shows rapid capacity decay, and after 50 cycles, the discharge capacity is dropped to 151 mAh g^{-1} compared with that of 714 mAh g^{-1} for the first cycle (Figure 3c). Figure 3d shows a green light-emitting diode being lit by the prototype cell using cobalt sulfide−$Li_7P_3S_{11}$ nanocomposites, indicating its promising practical applications in energy storage.

The intimate contact interface between cobalt sulfide and $Li_7P_3S_{11}$ electrolyte also greatly enhanced the rate capability of the cobalt sulfide−$Li_7P_3S_{11}$ nanocomposite electrode. Figure 4a shows the charge−discharge behavior of cobalt sulfide−$Li_7P_3S_{11}$ nanocomposite electrode under different current densities from 0.13 to 12.73 mA cm^{-2} after the first two aging cycles. The reversible discharge capacities for the cobalt sulfide−$Li_7P_3S_{11}$ nanocomposite electrode at 0.13, 0.38, 0.64, 1.27, 3.82, 6.37, and 12.73 mA cm^{-2} are 646, 623, 575, 501, 378, 266, and 152 mAh g^{-1}, respectively. In contrast, the capacities of the cobalt sulfide nanosheet electrode decays much more rapidly with increasing current density and the discharge capacity values at 0.13, 0.38, 0.64, 1.27, 3.82, and 6.37 mA cm^{-2} are only 560, 500, 331, 210, 89, and 34 mAh g^{-1}, respectively (Figure 4b). Obviously, the rate capability is greatly improved with the cooperation of $Li_7P_3S_{11}$ electrolyte. Figure 4c shows the relationship between the energy density and the average power density (Ragone plot). At low current density of 0.13 mA cm^{-2}, the cell show an energy density of 360 Wh kg^{-1}, calculated based on the total weight of cathode layer composed of cobalt sulfide−$Li_7P_3S_{11}$ nanocomposites and the neat $Li_7P_3S_{11}$ electrolyte as well as Super P, which is almost twice as high as that of $LiCoO_2$-based cathode in the solid-state lithium batteries.[8] In addition, at a very high current density of 12.73 mA cm^{-2}, the power density can be up to 3823 W kg^{-1}. The superior long-term cycling stability at a high current density of 1.27 mA cm^{-2} is further demonstrated in Figure 4d. Clearly, the cobalt sulfide−$Li_7P_3S_{11}$ nanocomposite electrode shows excellent cycling stability and the reversible discharge capacities can be maintained at 421 mAh g^{-1} after 1000 cycles, while for the cobalt sulfide nanosheet electrode, the discharge capacity is rapidly decreased with increasing cycle number and drops to 35 mAh g^{-1} at the 1000th cycle. These results indicate that excellent rate and cycling stability for all-solid-state lithium batteries employing cobalt sulfide−$Li_7P_3S_{11}$ nanocomposite electrode is realized.

To gain an insight into the improved electrochemical performances of the cobalt sulfide−$Li_7P_3S_{11}$ nanocomposites, the evolution of reaction kinetics at different charge−discharge cycles were analyzed using electrochemical impedance spectroscopy (EIS). As shown in Figure S10, both electrodes after the first cycle exhibit almost identical ohmic resistances due to using the same electrolyte bilayer and similar electrode layers. However, there are quite differences in the interfacial resistance between cobalt sulfide and $Li_7P_3S_{11}$ solid electrolytes. The cobalt sulfide−$Li_7P_3S_{11}$ nanocomposite electrode exhibits very small interfacial resistance, while that of the cobalt sulfide nanosheet electrode shows a larger semicircle resistance after the first cycle. After 1000 cycles, the cobalt sulfide−$Li_7P_3S_{11}$ nanocomposite electrode shows a much smaller increase in both ohmic resistance as well as the interfacial resistance than those of cobalt sulfide nanosheets. Indeed, the larger increase of the ohmic resistance and interfacial resistance of cobalt sulfide nanosheets probably attributes to the uneven volume expansion of cobalt sulfide sheets, resulting in cracking in both electrode and electrolyte bilayers. It is generally accepted that repeated lithiation−delithiation generates significant stresses and strains in the electrodes that ultimately lead to quick performance degradation during charge−discharge cycles, even in the flowable liquid electrolyte,[28,29] especially at a high charging and discharging rate.[30] The situation becomes much worse in the solid-state batteries due to impressable solid-state electrolytes. For cobalt sulfide−$Li_7P_3S_{11}$ nanocomposite electrode, due to the intimate contact between electrode and electrolyte, uniform volume change in cobalt sulfide−$Li_7P_3S_{11}$ nanocomposites can generate homogeneous volume change, resulting in small stress and strain in both electrode and electrolyte; thus, cobalt sulfide−$Li_7P_3S_{11}$ still retains integrated morphology even after 1000 cycles at 1.27 mA cm^{-2} (Figure S11a). In addition, the $Li_7P_3S_{11}$ particles still anchored on the surface of the cobalt sulfide sheets (Figure S11b). In sharp contrast, the point-to-point contact between the cobalt sulfide nanosheet and the $Li_7P_3S_{11}$ electrolyte in an uncoated cobalt sulfide nanosheet electrode result in a uneven volume change during lithiation and delithiation, resulting in huge stress and strain in both electrode and electrolyte and, thus, chemical and physical degradation of the electrode[31−33] and cracking in electrolytes. It can be seen that the electrode containing cobalt sulfide nanosheets after 1000 cycles shows intumescent surface (Figure S11c), and the cobalt sulfide nanosheets collapse without preserving an integrated electrode construction after long-term cycling (Figure S11d). The cracking in electrode and electrolyte layers result in the increase in ionic resistance as demonstrated by the increase the ohm resistance of the cell using uncoated cobalt sulfide nanosheet electrode from 151 ohm in the first cycle to 707 ohm in the 1000th cycle. Moreover, such inherently large volumetric expansion and contraction could absolutely cause detachment of the electrode materials from electrolytes, which also increase the interface resistance as evidenced in the increased semicircle size after 1000 cycles.

Clearly, the cobalt sulfide−$Li_7P_3S_{11}$ nanocomposites show remarkable electrochemical performances in all-solid-state lithium batteries, which could benefit from the following

DOI: 10.1021/acs.nanolett.6b03448
Nano Lett. 2016, 16, 7148−7154

aspects: (i) the anchored $Li_7P_3S_{11}$ coating not only endows a stable solid−solid contact interface between cobalt sulfide and sulfide electrolyte but also efficiently prevent the cracking or crumbling of electrode and electrolyte upon continuous cycling, thus maintaining high rate capability and cycling stability. (ii) The electrolyte in the cathode layer with reduced particle size and improved ionic conductivity could provide an intimate physical contact between active materials and electrolyte as well as fast lithium ions diffusion, leading to excellent power and cyclic performances. (iii) A solid electrolyte bilayer, i.e., $Li_{10}GeP_2S_{12}$ and 70% Li_2S−29% P_2S_5−1% P_2O_5, is used, avoiding the reaction between $Li_{10}GeP_2S_{12}$ and lithium metal and ensuring the compatibility between electrolyte and metallic lithium.[34] Thus, the implement of a lithium metal as an anode instead of its alloys could no doubt increase the energy density of the cell. (iv) The two-dimensional cobalt sulfide nanosheets could provide short pathways and high kinetics for lithium ion insertion and extraction due to their unique geometry with high surface-to-volume ratios,[35] resulting in a higher specific capacity. On the basis of the above analyses, it is clearly demonstrated that the unique interfacial architecture, i.e., an anchored $Li_7P_3S_{11}$ coating on cobalt sulfide nanosheets, and the novel neat $Li_7P_3S_{11}$ electrolyte within the cathode layer are responsible for the excellent electrochemical performances.

In summary, cobalt sulfide−sulfide electrolyte nanocomposites are successfully developed by an in situ liquid-phase method. The interfacial compatibility between cobalt sulfide and sulfide electrolyte is greatly improved by anchoring nanosized $Li_7P_3S_{11}$ electrolyte particles onto the surface of cobalt sulfide nanosheets. The unique interfacial structure endows intimate contact between electrode material and electrolyte, forming favorable lithium ion conduction paths at the interface and reducing the interfacial resistance, leading to ultrastable all-solid-state lithium batteries (421 mAh g^{-1} at 1.27 mA cm^{-2} after 1000 cycles) with high energy and power densities of 360 Wh kg^{-1} and 3823 W kg^{-1} at current densities of 0.13 and 12.73 mA cm^{-2}, respectively. This contribution demonstrates a new interfacial design for all-solid-state battery with high performances, which can be used as a generic route for synthesizing other sulfur-based or transitional metal sulfides−sulfide electrolyte composites for the all-solid-state lithium batteries.

■ ASSOCIATED CONTENT

Supporting Information

The Supporting Information is available free of charge on the ACS Publications website at DOI: 10.1021/acs.nanolett.6b03448.

Additional experimental details. Figures showing SEM, TEM, and HRTEM imaging of cobalt sulfide nanosheets; SEM and TEM images of cobalt sulfide−$Li_7P_3S_{11}$ nanocomposites; statistical particle size distribution of the anchored $Li_7P_3S_{11}$ electrolyte; Raman spectum of the neat $Li_7P_3S_{11}$ electrolyte; XRD patterns of sulfide electrolyte samples prepared by acetonitrile solvent; ionic conductivities of $Li_7P_3S_{11}$ sulfide electrolytes; dependence of conductivities on temperature for the neat $Li_7P_3S_{11}$ electrolytes; initial charge-discharge curves and cyclic performances of Li-In−neat $Li_7P_3S_{11}$ electrolyte−$LiCO_2$ all-solid-state cell under a current density of 0.1 C (1 C = 120 mA g^{-1}) at room temperature; an SEM image of the neat $Li_7P_3S_{11}$ electrolyte; schematic diagram of an all-solid-state lithium battery; Nyquist plots of cobalt sulfide−$Li_7P_3S_{11}$ nanocomposites and cobalt sulfide nanosheets after 1st and 1000th cycles at current density of 1.27 mA cm^{-2}; SEM images of cobalt sulfide−$Li_7P_3S_{11}$ nanocomposite and cobalt sulfide nanosheet electrodes after 1000 cycles; XRD pattern and SEM image of $Li_{10}GeP_2S_{12}$ electrolyte; and Nyquist plots of the $Li_{10}GeP_2S_{12}$ and 70% Li_2S−29% P_2S_5−1% P_2O_5 electrolytes at room temperature. A table showing ionic conductivities and activation energies of sulfide electrolytes prepared by various solvents for Li^+ ion conduction. (PDF)

■ AUTHOR INFORMATION

Corresponding Authors

*X.X. e-mail: xuxx@nimte.ac.cn.

*Y.-S.H. e-mail: yshu@iphy.ac.cn.

Author Contributions

X.Y. and D.L. contributed equally to this work.

Notes

The authors declare no competing financial interest.

■ ACKNOWLEDGMENTS

This work was supported by funding from the Strategic Priority Research Program of the Chinese Academy of Sciences (grant no. XDA09010201), the National Natural Science Foundation of China (grant no. 51502317), and the Key Scientific and Technological Innovation Team Project of Zhejiang province (grant no. 2013PT16). Dr. C. Wang would like to acknowledge the financial support from Army Research Office (Program Manager: Dr. Robert Mantz) under award no. W911NF1510187.

■ REFERENCES

(1) Tarascon, J. M.; Armand, M. *Nature* **2001**, *414*, 359−367.

(2) Wang, Y.; Richards, W. D.; Ong, S. P.; Miara, L. J.; Kim, J. C.; Mo, Y. F.; Ceder, G. *Nat. Mater.* **2015**, *14*, 1026−1032.

(3) Hu, Y.-S. *Nat. Energy* **2016**, *1*, 16042.

(4) Motavalli, J. *Nature* **2015**, *526*, S96−S97.

(5) Li, W. Y.; Yao, H. B.; Yan, K.; Zheng, G. Y.; Liang, Z.; Chiang, Y. M.; Cui, Y. *Nat. Commun.* **2015**, *6*, 7436.

(6) Qian, J. F.; Henderson, W. A.; Xu, W.; Bhattacharya, P.; Engelhard, M.; Borodin, O.; Zhang, J. G. *Nat. Commun.* **2015**, *6*, 6362.

(7) Kitaura, H.; Hayashi, A.; Tadanaga, K.; Tatsumisago, M. *J. Electrochem. Soc.* **2010**, *157*, A407−A411.

(8) Ohta, N.; Takada, K.; Zhang, L.; Ma, R.; Osada, M.; Sasaki, T. *Adv. Mater.* **2006**, *18*, 2226−2229.

(9) Kato, Y.; Hori, S.; Saito, T.; Suzuki, K.; Hirayama, M.; Mitsui, A.; Yonemura, M.; Iba, H.; Kanno, R. *Nat. Energy* **2016**, *1*, 16030.

(10) Kamaya, N.; Homma, K.; Yamakawa, Y.; Hirayama, M.; Kanno, R.; Yonemura, M.; Kamiyama, T.; Kato, Y.; Hama, S.; Kawamoto, K.; Mitsui, A. *Nat. Mater.* **2011**, *10*, 682−686.

(11) Kwon, O.; Hirayama, M.; Suzuki, K.; Kato, Y.; Saito, T.; Yonemura, M.; Kamiyama, T.; Kanno, R. *J. Mater. Chem. A* **2015**, *3*, 438−446.

(12) Sakuda, A.; Hayashi, A.; Tatsumisago, M. *Chem. Mater.* **2010**, *22*, 949−956.

(13) Takada, K. *Langmuir* **2013**, *29*, 7538−7541.

(14) Haruyama, J.; Sodeyama, K.; Han, L.; Takada, K.; Tateyama, Y. *Chem. Mater.* **2014**, *26*, 4248−4255.

(15) Tatsumisago, M.; Nagao, M.; Hayashi, A. *J. Asian Ceram. Soc.* **2013**, *1*, 17−25.

(16) Shin, B. R.; Nam, Y. J.; Kim, J. W.; Lee, Y.-G.; Jung, Y. S. *Sci. Rep.* **2014**, *4*, 5572.

DOI: 10.1021/acs.nanolett.6b03448
Nano Lett. 2016, 16, 7148−7154

(17) Aso, K.; Sakuda, A.; Hayashi, A.; Tatsumisago, M. *ACS Appl. Mater. Interfaces* **2013**, *5*, 686−690.
(18) Liu, Z.; Fu, W.; Payzant, E. A.; Yu, X.; Wu, Z.; Dudney, N. J.; Kiggans, J.; Hong, K.; Rondinone, A. J.; Liang, C. *J. Am. Chem. Soc.* **2013**, *135*, 975−978.
(19) Park, K. H.; Oh, D. Y.; Choi, Y. E.; Nam, Y. J.; Han, L.; Kim, J.-Y.; Xin, H.; Lin, F.; Oh, S. M.; Jung, Y. S. *Adv. Mater.* **2016**, *28*, 1874−1883.
(20) Zhou, Y. L.; Yan, D.; Xu, H. Y.; Feng, J. K.; Jiang, X. L.; Yue, J.; Yang, J.; Qian, Y. T. *Nano Energy* **2015**, *12*, 528−537.
(21) Rangasamy, E.; Liu, Z. C.; Gobet, M.; Pilar, K.; Sahu, G.; Zhou, W.; Wu, H.; Greenbaum, S.; Liang, C. D. *J. Am. Chem. Soc.* **2015**, *137*, 1384−1387.
(22) Ito, S.; Nakakita, M.; Aihara, Y.; Uehara, T.; Machida, N. *J. Power Sources* **2014**, *271*, 342−345.
(23) Adair, J. H.; Suvaci, E. *Curr. Opin. Colloid Interface Sci.* **2000**, *5*, 160−167.
(24) Gomez-Camer, J. L.; Martin, F.; Morales, J.; Sanchez, L. *J. Electrochem. Soc.* **2008**, *155*, A189−A195.
(25) Shi, W.; Zhu, J.; Rui, X.; Cao, X.; Chen, C.; Zhang, H.; Hng, H. H.; Yan, Q. *ACS Appl. Mater. Interfaces* **2012**, *4*, 2999−3006.
(26) Poizot, P.; Laruelle, S.; Grugeon, S.; Dupont, L.; Tarascon, J. M. *Nature* **2000**, *407*, 496−499.
(27) Ji, X.; Nazar, L. F. *J. Mater. Chem.* **2010**, *20*, 9821−9826.
(28) Tavassol, H.; Jones, E. M. C.; Sottos, N. R.; Gewirth, A. A. *Nat. Mater.* **2016**, DOI: 10.1038/nmat4708.
(29) Sun, Y.; Liu, N.; Cui, Y. *Nat. Energy* **2016**, *1*, 16071.
(30) Ning, G.; Haran, B.; Popov, B. N. *J. Power Sources* **2003**, *117*, 160−169.
(31) Ebner, M.; Marone, F.; Stampanoni, M.; Wood, V. *Science* **2013**, *342*, 716−720.
(32) Mukhopadhyay, A.; Sheldon, B. W. *Prog. Mater. Sci.* **2014**, *63*, 58−116.
(33) Jiang, J.; Zhu, J.; Ai, W.; Wang, X.; Wang, Y.; Zou, C.; Huang, W.; Yu, T. *Nat. Commun.* **2015**, *6*, 8622.
(34) Wan, H.; Peng, G.; Yao, X.; Yang, J.; Cui, P.; Xu, X. *Energy Storage Mater.* **2016**, *4*, 59−65.
(35) Chhowalla, M.; Shin, H. S.; Eda, G.; Li, L.-J.; Loh, K. P.; Zhang, H. *Nat. Chem.* **2013**, *5*, 263−275.

DOI: 10.1021/acs.nanolett.6b03448
Nano Lett. 2016, 16, 7148−7154